

New charge exchange model of GEANT4 for ${}^9\text{Be}(\text{p},\text{n}){}^9\text{B}$ reaction

Jae Won Shin

Department of Physics, Sungkyunkwan University, Suwon 440-746, Korea

Tae-Sun Park

Department of Physics, Sungkyunkwan University, Suwon 440-746, Korea

Abstract

A new data-based charge exchange model of GEANT4 dedicated to the ${}^9\text{Be}(\text{p},\text{n}){}^9\text{B}$ reaction is developed by taking the ENDF/B-VII.1 differential cross-section data as input. Our model yields results that are in good agreement with the experimental neutron yield spectrum data obtained for proton beams of energy (20 ~ 35) MeV. In particular, in contrast to all the considered GEANT4 hadronic models, the peak structure resulting from the discrete neutrons generated by the charge-exchange reaction is observed to be accurately reproduced in our model.

Keywords: GEANT4, ${}^9\text{Be}(\text{p},\text{n}){}^9\text{B}$, neutron yield, ENDF/B-VII.1

PACS: 25.40.-h, 24.10.Lx, 02.70.Uu

1. Introduction

Neutron sources play essential roles in various industrial and scientific fields. In obtaining neutron beams with the desired energy spectrum, one approach that is commonly adopted is the use of neutron-emitting radio isotopes, such as ${}^{252}\text{Cf}$ and Be-coupled ${}^{241}\text{Am}$. In this method, however, the

Email address: tspark@kias.re.kr (Tae-Sun Park)

energies of the neutrons are on the order of a few MeV and are determined by the isotope. That is, the neutron spectra of ^{252}Cf and $^{241}\text{Am-Be}$ are smooth curves with average energies of ~ 2.2 MeV and ~ 4.5 MeV, respectively, and thus, they are not suitable when more energetic neutrons are required.

A more flexible method is to bombard proton beams on a target; in this case, neutrons are generated mainly through the (p,n) charge exchange reaction. By adjusting the beam energy, the target material and the thickness of the target, the resulting neutron spectrum can be controlled to a certain degree. Beryllium is widely used as the target material due to its high melting point, good thermal conductivity and many other desired features. Creating particle transport codes to accurately reproduce the neutron energy spectrum of the $^9\text{Be(p,n)}^9\text{B}$ reaction is thus of great importance.

For proton beams of energy ($20 \sim 35$) MeV impinged on a 0.1 cm thick beryllium target, we first performed a comparative study with GEANT4 [1, 2] and PHITS [3], and observed that all the platforms substantially underestimate the neutron yields (\mathcal{Y}_n).¹ This finding may not be too surprising because the hadronic models of the platforms have been developed for wide use, but none of the models is specialized for the $^9\text{Be(p,n)}^9\text{B}$ reaction.

In this work, we developed a charge exchange model of GEANT4 dedicated to the $^9\text{Be(p,n)}^9\text{B}$ reaction, taking the ENDF/B-VII.1 differential cross-section data [6] as input. When combined with the G4BinaryCascade [7] model for continuum neutrons, the developed model is observed to accurately describe the experimental neutron yield spectra, see Figs. 8 and 10. In particular, the peak structure due to the discrete neutrons is well repro-

¹There are also MCNPX [4] simulation results for 11 MeV protons impinged on a 0.2 cm thick beryllium target [5]. The simulations show that although rather good agreement is achieved overall, the model overestimates the neutron yield near the end point (e.g., $E_n \simeq 9$ MeV at forward angle).

duced, whereas all other considered models are highly problematic in this respect.

2. Simulation tool

GEANT4 is a tool kit that allows for microscopic Monte Carlo simulations of particles interacting with materials. The platform has been thoroughly tested and is widely used in many different scientific fields, such as medical physics [8, 9, 10], accelerator-based radiation studies [11, 12, 13], neutron shielding studies [14, 15, 16], and environment radiation detection [17, 18, 19].

In this work, we simulated the neutrons produced by proton beams on a ^9Be target by using GEANT4 v10.0. For the electromagnetic processes, we adopted “G4EmStandardPhysics_option3”. For the hadronic inelastic processes, four different hadronic models were considered: “G4BertiniCascade” [20], “G4BinaryCascade” [7], “G4Precompound” [21] and “G4INCLCascade” [22], which will be hereafter referred to as “G4BERTI”, “G4BC”, “G4PRECOM” and “G4INCL”, respectively. The models are described in detail in the Physics Reference Manual [23] and Refs. [24, 25].

3. Results

3.1. Benchmarking simulations

As mentioned in the Introduction, GEANT4 is not equipped with a specialized routine for the $^9\text{Be}(p,n)^9\text{B}$ reaction. To quantify the accuracy of the hadronic models of GEANT4, we simulated the neutron yields due to 35 MeV protons directed toward a 0.1 cm thick Be target, whose experimental data are presented in Ref. [26] and in the EXFOR database [27]. According to the experimental setup, the diameter of the proton beam was set to 0.4 cm (with a flat shape), and we placed a cylindrical scoring geometry measuring 0.1 cm in thickness and 5.1 cm in diameter at a distance of 1.3 m from the

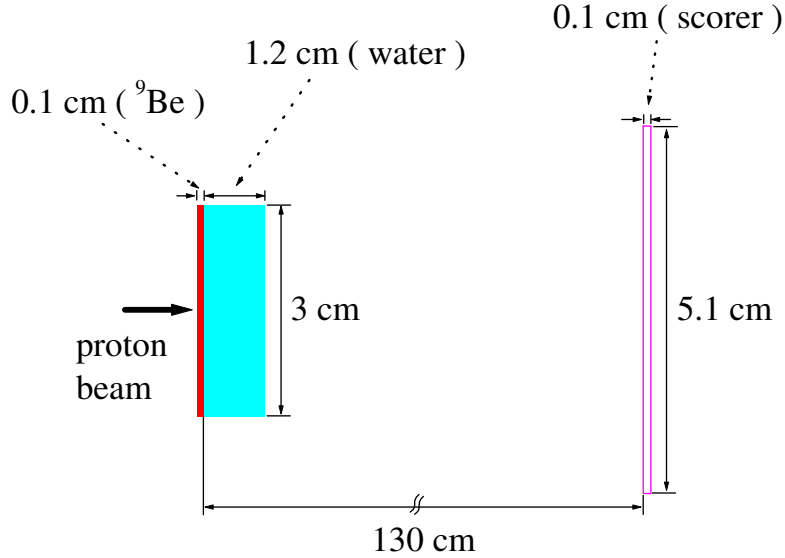


Figure 1: (Color online) Schematic diagram of the simulation geometry.

target; see Fig. 1 for the simulation geometry. We also took into account the proton stopper of the experiment, *i.e.*, the 1.2 cm thick water layer placed behind the target. We repeated our simulations for each of the four hadronic models mentioned above.

Figure 2 shows the neutron energy spectra in the forward angle, $\theta_{\text{lab}} = 0^\circ$, where E_p and E_n represent for the energy of the incident protons and the outgoing neutrons, respectively. The figure clearly shows that the considered models do not reproduce the peak structure at $E_n \simeq 32$ MeV, where the peak is mainly due to discrete neutrons produced by the $^9\text{Be}(p,n)^9\text{B}$ reaction.

To confirm our findings, we simulated the total and angular differential cross-sections of the $^9\text{Be}(p,n)^9\text{B}$ reaction. The results are presented in Fig. 3, which indicate that enormous discrepancies exist among the models; indeed,

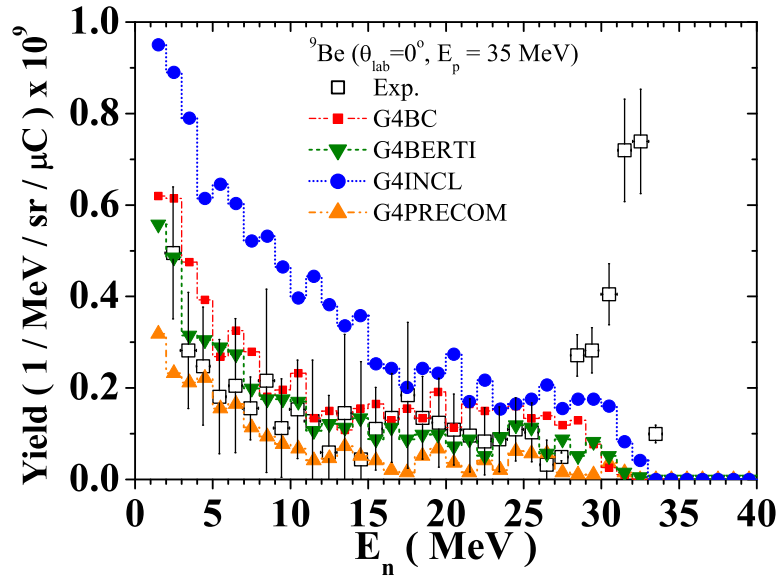


Figure 2: (Color online) Energy spectra of neutrons at $\theta_{\text{lab}} = 0^\circ$ produced by 35 MeV protons on a 0.1 cm ^9Be target. The open squares represent the experimental data [26], the red squares G4BC, the green inverted triangles G4BERTI, the blue circles G4INCL and the orange triangles G4PRECOM.

none of the models is in agreement with the ENDF/B-VII.1 data.² To gain a better microscopic understanding, we also plotted the double differential cross-sections with respect to the neutron energy in the forward angle, as shown in Fig. 4. The figure clearly shows that the GEANT4 hadronic models (Fig. 4 (a)) fail to describe the sharp peak structure of the ENDF/B-VII.1 data (Fig. 4 (b)).

Indeed, without the peak structure, it is not possible to describe the neutron spectrum accurately. Therefore, we constructed a GEANT4 hadronic model dedicated to the ${}^9\text{Be}(p,n){}^9\text{B}$ reaction, a detailed description of which is presented in the next section.

3.2. ${}^9\text{Be}(p,n){}^9\text{B}$ charge exchange model

It should be noted that there is a GEANT4 hadronic model for charge exchange reactions, G4ChargeExchange (“G4CE”). To demonstrate the accuracy of the model, we repeated the simulation under the same conditions described above. Noting that G4CE covers only the charge-exchange reaction but not other continuum neutrons, we studied three cases, G4CE, G4BC and G4BC+G4CE. For the G4BC+G4CE case, to avoid any possible double counting, we removed the neutrons produced by the ${}^9\text{Be}(p,n){}^9\text{B}$ reaction of G4BC for the entire energy region by making use of the G4UserSteppingAction class. The resulting neutron yields are plotted in Fig. 5, which shows that adding G4CE on top of G4BC improves the accuracy remarkably. However, an error of approximately 20% in the height for the n_0 peak remains, and the n_i ($i \geq 1$) peaks are still missing, where n_0 and n_i denote the neutrons with the residual ${}^9\text{B}$ in the ground and i -th excited states, respectively.

² In extracting the ENDF/B-VII.1 differential cross-section values, we combined the ENDF MF=3 and MF=6 data using a software program that is currently under development [28, 29].

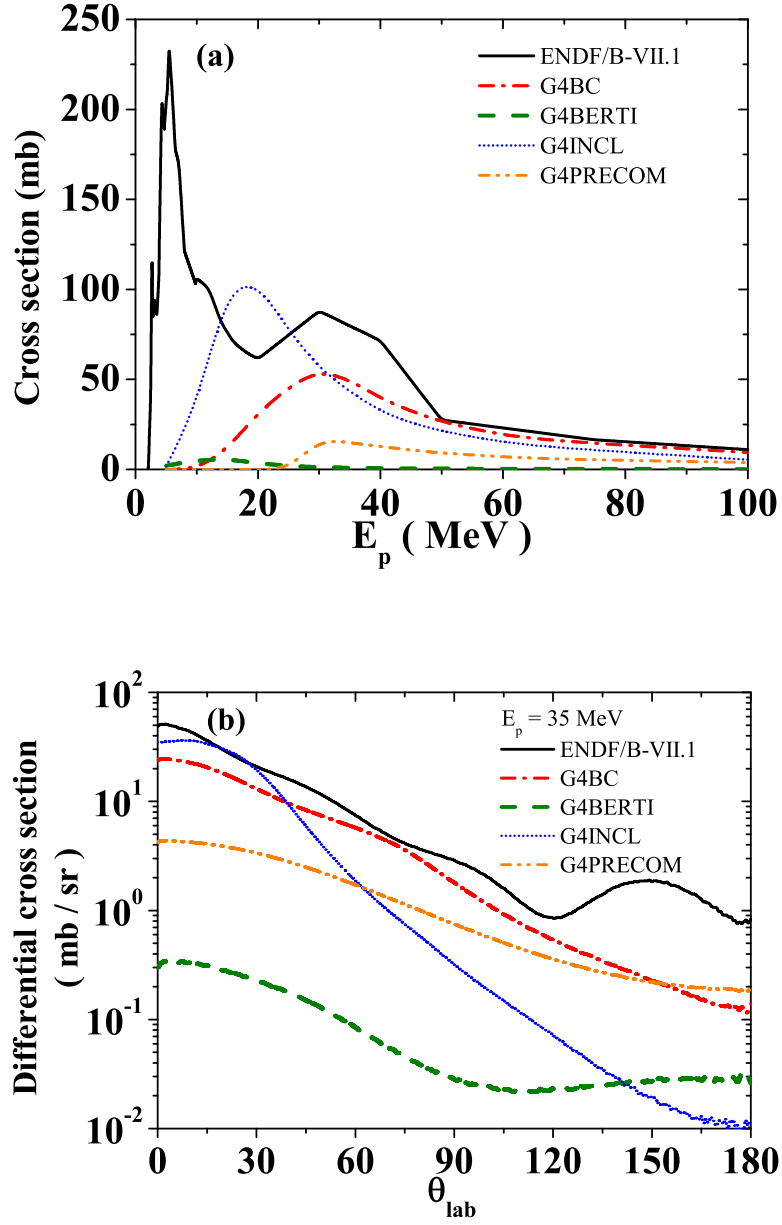


Figure 3: (Color online) Total cross-sections with respect to the incident proton energy (a) and the differential cross-sections with respect to the angle θ_{lab} at $E_p = 35$ MeV (b) of the ${}^9\text{Be}(p,n){}^9\text{B}$ reaction.

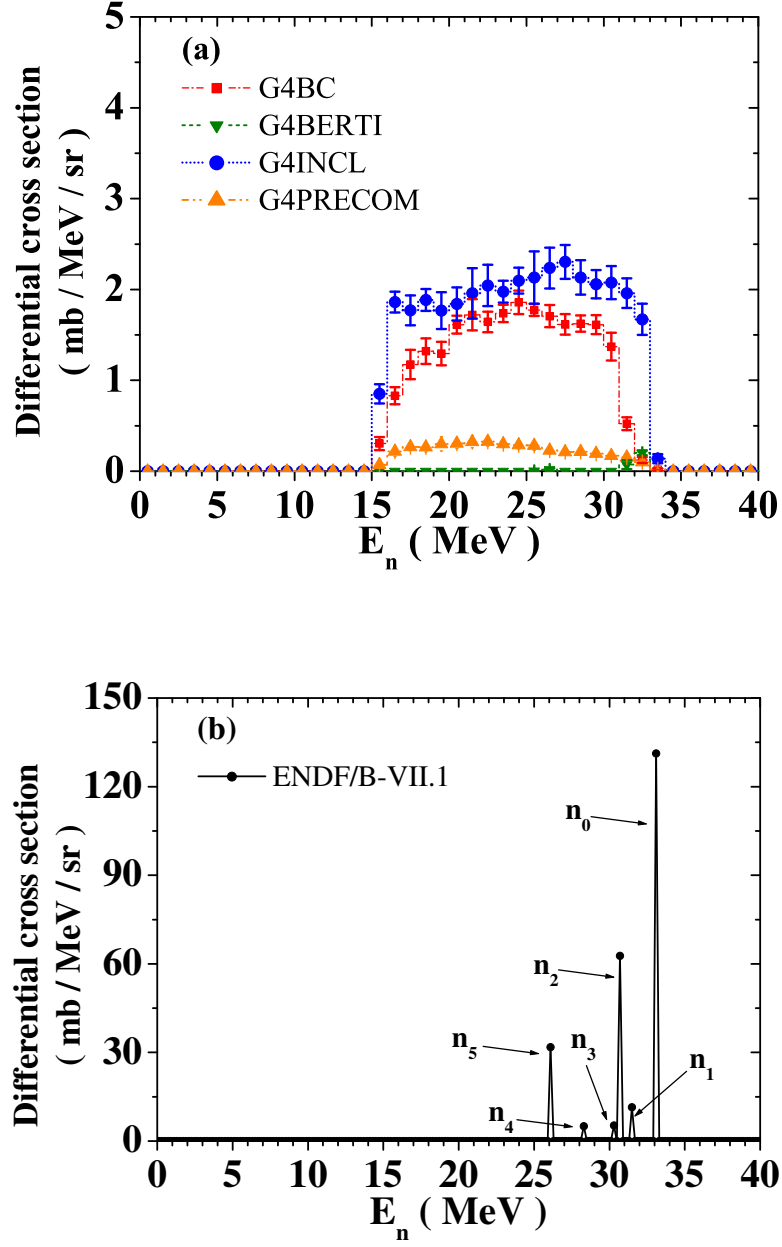


Figure 4: (Color online) Double differential cross-sections with respect to neutron energy at $\theta_{lab} = 0^\circ$. (a) and (b) show the results obtained from the models of GEANT4 and ENDF/B-VII.1, respectively.

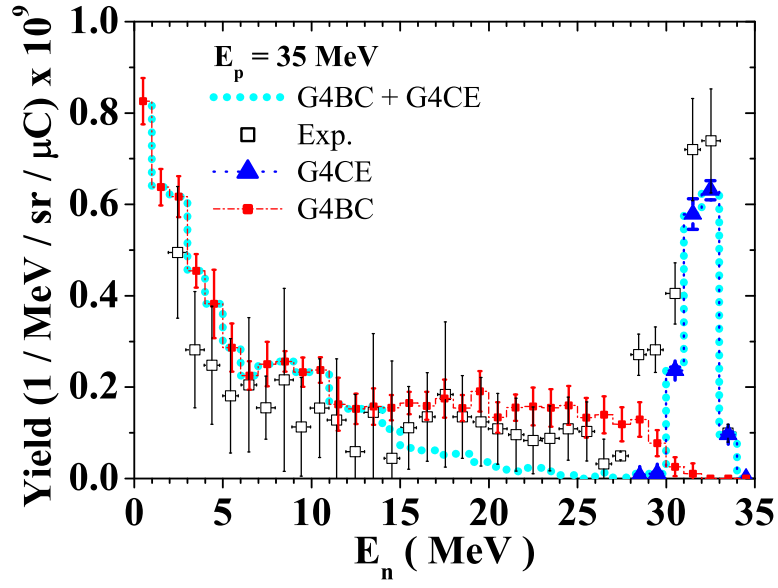


Figure 5: (Color online) Energy spectra of neutron yields at $\theta_{\text{lab}} = 0^\circ$ for 35 MeV protons on a 0.1 cm ^9Be target. The open squares, the blue triangles and the red squares represent the experimental data [26], the G4CE results and the G4BC results, respectively. The dotted line represents the values of \mathcal{Y}_n calculated using G4BC + G4CE.

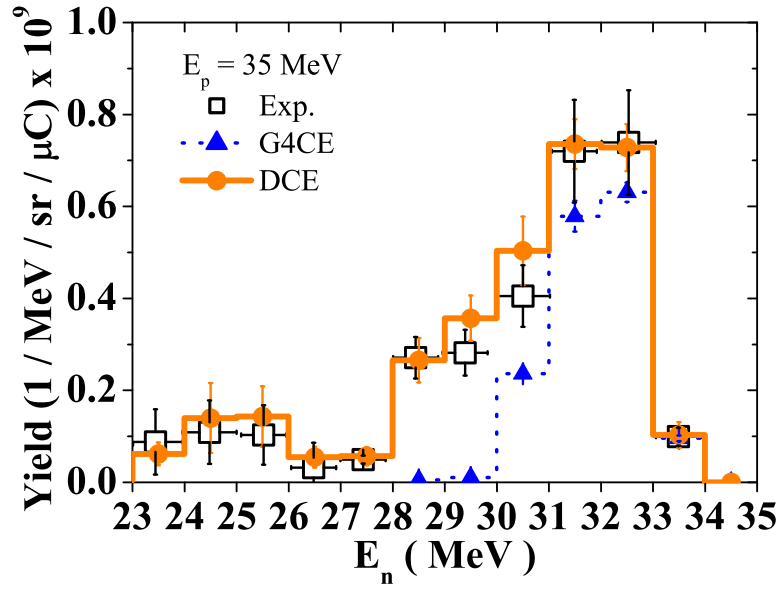


Figure 6: (Color online) Neutron energy spectra at $\theta_{\text{lab}} = 0^\circ$ produced by 35 MeV protons. The open squares represent the experimental data [26], the blue triangles with a dotted line represent the G4CE results, and the orange circles with a solid line represent the results of our DCE model.

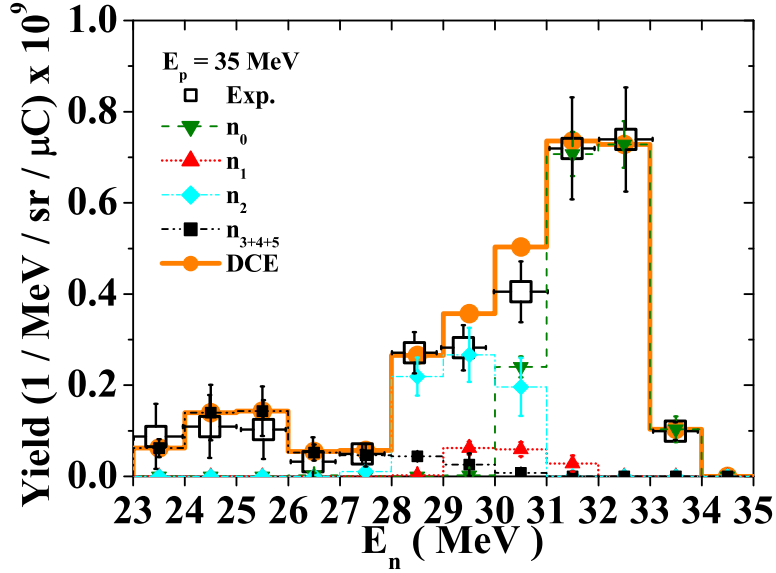


Figure 7: (Color online) Neutron energy spectra at $\theta_{\text{lab}} = 0^\circ$ produced by 35 MeV protons on a ^9Be target. The open squares represent the experimental data [26]. The green inverted triangles, the red triangles, the cyan diamonds and the black squares denote the calculated values of n_0 , n_1 , n_2 and $n_3+n_4+n_5$, respectively, and the orange circles with a solid line represent the results of our DCE model.

For an accurate description of discrete neutrons, we developed a data-based charge exchange (DCE) model. For the discrete neutrons from the $^9\text{Be}(p,n)^9\text{B}$ reaction, the ENDF/B-VII.1 differential cross-section data [6] of the reaction were taken as input. The resulting \mathcal{Y}_n is plotted in Fig. 6, which shows that the prediction of the DCE model is in good agreement with the experimental data.

The contribution of each n_i to the yield is plotted in Fig. 7, which shows that the contribution of n_2 is quite substantial, without which the shoulder of the peak cannot be reproduced. In contrast, the contributions of n_1 and n_i , with $i \geq 3$, are observed to be marginal. The figure also shows that the width of each peak is approximately 3 MeV, which is mainly due to the energy loss

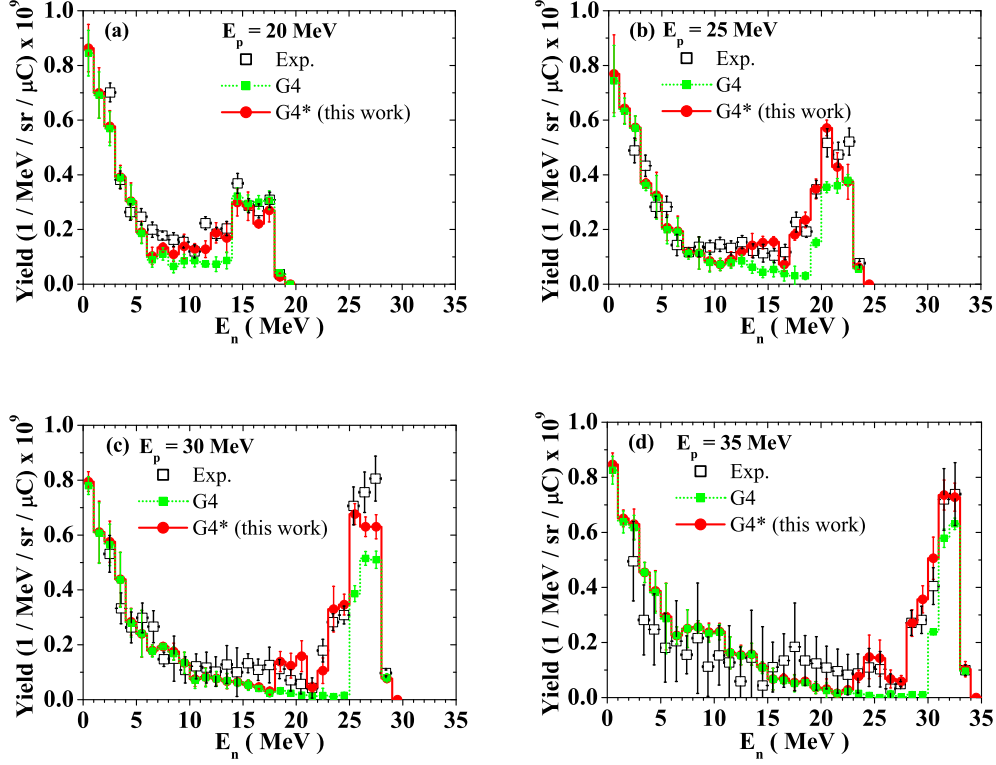


Figure 8: (Color online) Neutron energy spectra at $\theta_{\text{lab}} = 0^\circ$ produced by 20, 25, 30 and 35 MeV incident proton beams on a ^9Be target are plotted in (a), (b), (c) and (d), respectively. The open squares shown in black are the experimental data [26]. The green squares with dotted lines and the red circles with solid lines denote the values of \mathcal{Y}_n calculated using G4 (G4BC + G4CE) and G4* (G4BC + DCE), respectively.

of the incident protons. For 35 MeV protons, the calculated average energy loss of the incident protons in the 0.1 cm thick ^9Be target is 2.58 ± 0.13 MeV, and the attenuation of the neutron energy due to the 1.2 cm thick water placed behind the target is approximately 0.2 MeV.

In addition to the discrete neutrons that are responsible for the peaks, continuum neutrons also appear in the low-energy region. Figure 2 and Fig. 5 show that the latter can be well described by G4BC. We thus combined G4BC with our DCE model to cover the neutron yield spectrum for the entire energy region; the resulting G4BC + DCE model is referred to as G4*. The

Table 1: The calculated-to-experimental ratio for the total neutron yields.

E_p (MeV)	G4BC	G4BC+G4CE	this work
20	0.67 ± 0.05	0.77 ± 0.03	0.84 ± 0.04
25	0.70 ± 0.05	0.71 ± 0.03	0.99 ± 0.04
30	0.67 ± 0.04	0.67 ± 0.03	0.97 ± 0.04
35	0.82 ± 0.04	0.84 ± 0.04	1.13 ± 0.05

results of our combined G4* model for the neutron spectra produced by 20, 25, 30 and 35 MeV proton beams impinging on a 0.1 cm thick ^9Be target at $\theta_{\text{lab}} = 0^\circ$ are plotted in Fig. 8. A comparison of this figure with Fig. 2 reveals that the agreement with the experimental data near the peak region – where the $^9\text{Be}(p,n)^9\text{B}$ reaction plays a dominant role – is significantly improved. Below the peak region, the models show a tendency to underestimate the neutron yields, although their predictions are within the error of the data; see, for example, the $E_n = (15 \sim 24)$ MeV region for $E_p = 35$ MeV plotted in Fig. 8 (d). This discrepancy may derive from the inaccuracy in treating the continuum neutrons emanating from other reaction channels, such as $^9\text{Be}(p,pn)^8\text{Be}$ and $^9\text{Be}(p,n\alpha)^5\text{Li}$.

The calculated-to-experimental (C/E) ratios for the total and peak neutron yields are tabulated in Table 1 and Table 2, respectively. Table 1 shows that the error in the C/E ratio of G4BC for the total neutron yield is approximately 30 %, which is not particularly different from the error yielded by the G4CE model. However, when our DCE model is added, the error is reduced to approximately (0 ~ 16) %. The improvement for the peak neutrons is observed to be more dramatic. That is, the results of G4BC – which hardly covers the discrete neutrons that are responsible for the peaks – are completely unacceptable. By adding the G4CE model on top of the G4BC model, the error in the C/E ratio is reduced to (21 ~ 48) %. Moreover, by replacing the G4CE model with our DCE model, the error is further reduced

Table 2: The calculated-to-experimental ratio for the peak neutron yield, where the peak region of each E_p is denoted in the 2nd column.

E_p (MeV)	E_n (MeV) (peak region)	G4BC	G4BC+G4CE	this work
20	11 \sim 19	0.38 ± 0.04	0.79 ± 0.04	0.84 ± 0.06
25	17 \sim 24	0.20 ± 0.03	0.59 ± 0.02	0.96 ± 0.05
30	22 \sim 29	0.14 ± 0.03	0.52 ± 0.02	0.94 ± 0.04
35	28 \sim 34	0.10 ± 0.03	0.67 ± 0.02	1.16 ± 0.06

to (4 \sim 16) %.

The fraction of each peak contribution is plotted in Fig. 9, which shows the relative importance of the peaks. At $E_p = 35$ MeV, the fractions of n_0 , n_1 , n_2 and n_{3+4+5} are approximately 66%, 5.6%, 25% and 3%, respectively, and the G4BC contribution is observed to be negligibly small ($\sim 0.3\%$). The importance of continuum neutrons, however, increases at low proton beam energies, covering approximately 20% of the peak yield at $E_p = 20$ MeV.

We also performed PHITS simulations under the same conditions, exploring three hadronic models of PHITS, INCL [30, 31], Bertini [30] and QMD [30]. The results are plotted in Fig. 10. Below the peak region (e.g., $E_n \lesssim 24$ MeV), all the models are consistent with the data, taking into account the large experimental error bars. However, only the Bertini model of PHITS reproduces the peak structure, and the general behavior of the model is rather similar to that of the G4BC+G4CE model.

4. Conclusion

We examined several hadronic models of GEANT4 for the neutrons produced by proton beams impinging on a ^9Be target and observed that none of the models reproduces the peak structure of the neutron spectrum. Because the peak structure is due to the discrete neutrons generated by the $^9\text{Be}(p,n)^9\text{B}$ reaction, this finding suggests that the reaction is not properly

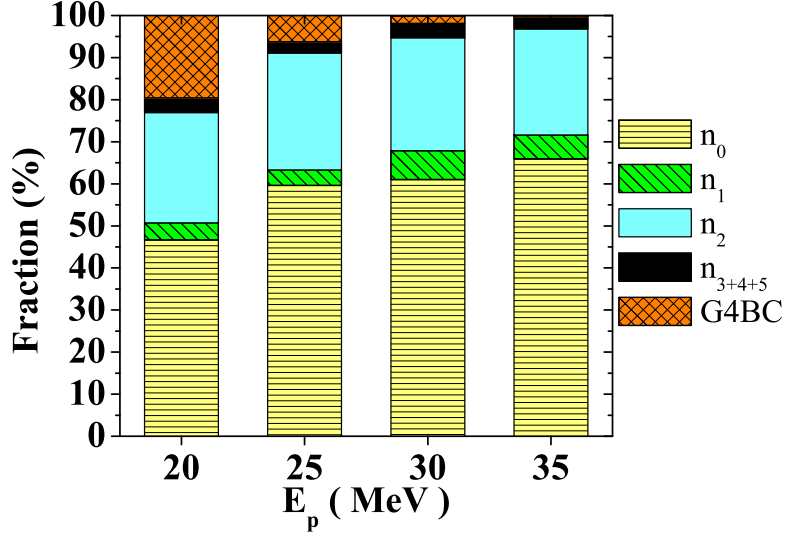


Figure 9: (Color online) Fraction of each contribution for the calculated peak neutron yield.

implemented in the models considered.

The charge exchange model of GEANT4, G4CE, was also studied; it was observed that the model reproduces the n_0 peak, but its height is reduced to approximately 80%, and n_i peaks with $i \geq 1$ remain missing. To eliminate this discrepancy, we developed a new data-based GEANT4 model dedicated to the ${}^9\text{Be}(p,n){}^9\text{B}$ reaction by incorporating ENDF/B-VII.1 differential cross-section data of the reaction into G4CE. For proton beams of energy $E_p = (20 \sim 35)$ MeV, the resulting model predictions are in good agreement with the experimental data. We also observed that noticeable discrepancies persist below the peak region. For an accurate reproduction of the neutron yields for the entire energy region, it is extremely important to extend our work to take into account the ENDF data of all the $p + {}^9\text{Be}$ channels, which is currently in progress.

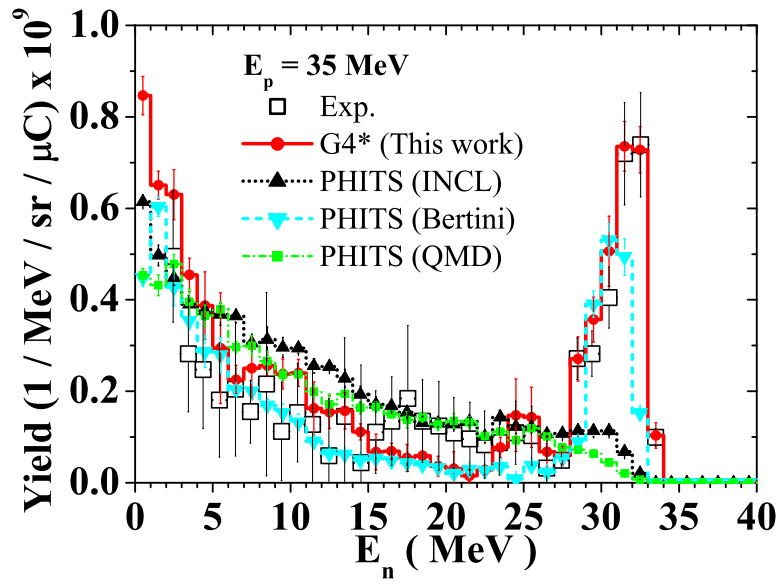


Figure 10: (Color online) Neutron energy spectra at $\theta_{\text{lab}} = 0^\circ$ for 35 MeV protons on a ^9Be target. The open squares shown in black represent the experimental data [26], and the red solid line with circles represents the G4* (G4BC + DCE) results. The black dotted line with triangles, the cyan dashed line with inverted triangles and the green long-dashed line with squares represent the results obtained by the PHITS calculation using the INCL, Bertini and QMD models, respectively.

Acknowledgments

This work was supported in part by the Basic Science Research Program through the Korea Research Foundation (NRF-2011-0025116, NRF-2012R1A1A2007826, NRF-2013R1A1A2063824).

References

- [1] S. Agostinelli, et al., GEANT4—a simulation toolkit, Nucl. Instrum. Meth. A 506 (2003) 250–303. doi:10.1016/S0168-9002(03)01368-8.
- [2] J. Allison, et al., Geant4 developments and applications, IEEE Trans. Nucl. Sci. 53 (2006) 270–278. doi:10.1109/TNS.2006.869826.
- [3] T. Sato, K. Niita, N. Matsuda, S. Hashimoto, Y. Iwamoto, S. Noda, T. Ogawa, H. Iwase, H. Nakashima, T. Fukahori, K. Okumura, T. Kai, S. Chiba, T. Furuta, L. Sihver, Particle and Heavy Ion Transport Code System PHITS, Version 2.52, J. Nucl. Sci. Technol. 50 (2013) 913–923. doi:10.1080/00223131.2013.814553.
- [4] Monte Carlo Code MCNPX: Los Alamos National Laboratory, Available online at <https://mcnp.lanl.gov/> .
- [5] S. Kamada, T. Itoga, Y. Unno, W. Takahashi, T. Oishi, M. Baba, Measurement of Energy-angular Neutron Distribution for ${}^7\text{Li}$, ${}^9\text{Be}(\text{p},\text{xn})$ Reaction at $\text{EP} = 70 \text{ MeV}$ and 11 MeV , J. Korean Phys. Soc. 59 (2011) 1676–1680. doi:10.3938/jkps.59.1676.
- [6] ENDF/B-VII.1, Available online at <http://www.nndc.bnl.gov/csewg/> .
- [7] G. Folger, V. N. Ivanchenko, J. P. Wellisch, The Binary Cascade, Eur. Phys. J. A 21 (2004) 407–417. doi:10.1140/epja/i2003-10219-7.

- [8] M. U. Bug, E. Gargioni, S. Guatelli, S. Incerti, H. Rabus, R. Schulte, A. B. Rosenfeld, Effect of a magnetic field on the track structure of low-energy electrons: a Monte Carlo study, *Eur. Phys. J. D* 60 (2010) 85–92. doi:10.1140/epjd/e2010-00145-1.
- [9] J. W. Shin, S.-W. Hong, C.-I. Lee, T.-S. Suh, Application of a GEANT4 Simulation to a ^{60}Co Therapy Unit, *J. Korean Phys. Soc.* 59 (2011) 12–19. doi:10.3938/jkps.59.12.
- [10] C. I. Lee, J. W. Shin, S.-C. Yoon, T. S. Suh, S.-W. Hong, K. J. Min, S. D. Lee, S. M. Chung, J.-Y. Jung, Percentage depth dose distributions in inhomogeneous phantoms with lung and bone equivalent media for small fields of CyberKnife (2014). arXiv:1401.0692.
- [11] J. K. Park, S. Kwon, S. W. Lee, J. T. Kim, J.-S. Chai, J. W. Shin, S.-W. Hong, Analysis of Single-event Upset for SRAM Devices by Using the MC-50 Cyclotron, *J. Korean Phys. Soc.* 58 (2011) 1511–1517. doi:10.3938/jkps.58.1511.
- [12] J. W. Shin, T.-S. Park, S. W. Hong, J. K. Park, J. T. Kim, J.-S. Chai, Estimates of SEU for Semiconductors Using MC50 Cyclotron and Geant4 Simulation, *J. Korean Phys. Soc.* 59 (2011) 2022–2025. doi:10.3938/jkps.59.2022.
- [13] Y. Malyshkin, I. Pshenichnov, I. Mishustin, T. Hughes, O. Heid, W. Greiner, Neutron production and energy deposition in fissile spallation targets studied with Geant4 toolkit, *Nucl. Instrum. Meth. B* 289 (2012) 79–90. doi:10.1016/j.nimb.2012.07.023.
- [14] S. Avery, C. Ainsley, R. Maughan, J. McDonough, Analytical shielding

- calculations for a proton therapy facility, *Radiat. Protect. Dosim.* 131 (2008) 167–179. doi:10.1093/rpd/ncn136.
- [15] S. I. Bak, T.-S. Park, S.-W. Hong, J. W. Shin, I. S. Hahn, Geant4 simulation of the shielding of neutrons from ^{252}Cf source, *J. Korean Phys. Soc.* 59 (2011) 2071–2074. doi:10.3938/jkps.59.2071.
- [16] J. W. Shin, S.-W. Hong, S.-I. Bak, D. Y. Kim, C. Y. Kim, GEANT4 and PHITS simulations of the shielding of neutrons from the ^{252}Cf source, *J. Korean Phys. Soc.* 65 (2014) 591–598. doi:10.3938/jkps.65.591.
- [17] S. Hurtado, M. García-León, R. García-Tenorio, GEANT4 code for simulation of a germanium gamma-ray detector and its application to efficiency calibration, *Nucl. Instrum. Meth. A* 518 (2004) 764–774. doi:10.1016/j.nima.2003.09.057.
- [18] K. Banerjee, et al., Variation of neutron detection characteristics with dimension of BC501A neutron detector, *Nucl. Instrum. Meth. A* 608 (2009) 440–446. doi:10.1016/j.nima.2009.07.034.
- [19] P. M. Joshirao, J. W. Shin, C. K. Vyas, A. D. Kulkarni, H. Kim, T. Kim, S.-W. Hong, V. K. Manchanda, Development of optical monitor of alpha radiations based on CR-39, *Appl. Radiat. Isot.* 81 (2013) 184–189. doi:10.1016/j.apradiso.2013.06.012.
- [20] A. Heikkinen, N. Stepanov, J. P. Wellisch, Bertini intra-nuclear cascade implementation in Geant4, *Computing in High Energy and Nuclear Physics 2003 Conference Proceedings* (2003). arXiv:nuc1-th/0306008.
- [21] K. K. Gudima, S. G. Mashnik, V. D. Toneev, Cascade-exciton model of nuclear reactions, *Nucl. Phys. A* 401 (1983) 329–361. doi:10.1016/0375-9474(83)90532-8.

- [22] A. Boudard, J. Cugnon, J.-C. David, S. Leray, D. Mancusi, New potentialities of the Liège intranuclear cascade (INCL) model for reactions induced by nucleons and light charged particles (2012). [arXiv:1210.3498](#).
- [23] GEANT4 Physics Reference Manual, Available online at <http://geant4.web.cern.ch/geant4/support/index.shtml> .
- [24] J. Apostolakis, et al., Progress in hadronic physics modelling in Geant4, J. Phys.: Conf. Ser. 160 (2009) 012073, XIII Int. Conf. on Calorimetry in High Energy Physics (CALOR 2008). [doi:10.1088/1742-6596/160/1/012073](#).
- [25] J. Yarba, Recent Developments and Validation of Geant4 Hadronic Physics, J. Phys.: Conf. Ser. 396 (2012) 022060, Int. Conf. on Computing in High Energy and Nuclear Physics 2012 (CHEP2012). [doi:10.1088/1742-6596/396/2/022060](#).
- [26] Y. Uwamino, T. Ohkubo, A. Torii, T. Nakamura, Semi-monoenergetic neutron field for activation experiments up to 40 MeV, Nucl. Instrum. Meth. A 271 (1988) 546–552. [doi:10.1016/0168-9002\(88\)90318-X](#).
- [27] EXFOR database, Available online at <http://www.nea.fr/html/dbdata/> .
- [28] S. I. Bak, R. Brun, F. Carminati, J. S. Chai, A. Gheata, M. Gheata, S.-W. Hong, Y. Kadi, V. Manchanda, T.-S. Park, C. Tenreiro, A New Format for Handling Nuclear Data, J. Korean Phys. Soc. 59 (2011) 1111–1114. [doi:10.3938/jkps.59.1111](#).
- [29] T.-S. Park, “TNudy project”, unpublished.

- [30] K. Niita, N. Matsuda, Y. Iwamoto, H. Iwase, T. Sato, H. Nakashima, Y. Sakamoto, L. Sihver, PHITS: Particle and Heavy Ion Transport code System, Version 2.23, JAEA-Data/Code 2010-022 (2010), Available online at <http://jolissrch-inter.tokai-sc.jaea.go.jp/pdfdata/JAEA-Data-Code-2010-022.pdf> (2010).
- [31] J. Cugnon, D. Mancusi, A. Boudard, S. Leray, New Features of the INCL4 Model for Spallation Reactions, J. Korean Phys. Soc. 59 (2011) 955–958. doi:10.3938/jkps.59.955.